RSC Advances

PAPER

View Article Online
View Journal | View Issue

Cite this: *RSC Adv.*, 2021, **11**, 10540

A novel route to size-controlled MIL-53(Fe) metal–organic frameworks for combined chemodynamic therapy and chemotherapy for cancer†

Anxia Li,[a] Xiaoxin Yang[b] and Juan Chen *[a]

Metal–organic frameworks (MOFs), such as MIL-53(Fe), have considerable potential as drug carriers in cancer treatment due to their notable characteristics, including controllable particle sizes, high catalytic activity, biocompatibility and large porosity, and are widely used in a broad range of drugs. In this study, a new approach for the synthesis of MIL-53(Fe) nanocrystals with controlled sizes has been developed using a non-ionic surfactant PVP as the conditioning and stabilizing agent, respectively. During the nucleation of MIL-53(Fe), the PVP droplet, as a nano-reactor, controlled the growth of the crystal nucleus. The size and aspect ratio (length/width) of nanocrystals increased with an increase in PVP in the synthetic mixture. The MIL-53(Fe) nanocrystals showed a homogeneous morphology, with approximately 190 nm in length and 100 nm in width. MIL-53(Fe) not only was used to load the anticancer drug doxorubicin (DOX) but also generated hydroxyl radicals (˙OH) *via* a Fenton-like reaction for ROS-mediated/chemo-therapy of cancer cells. The approach was expected to synthesize numerous types of nano-size iron(III)-based MOFs, such as MIL-53, 89, 88A, 88B and 101. The MIL-53(Fe) nanocrystals hold great promise as a candidate to improve the controlled release of drugs and treatment effect for cancer therapy.

Received 23rd November 2020
Accepted 19th February 2021

DOI: 10.1039/d0ra09915e

rsc.li/rsc-advances

Introduction

In recent years, metal–organic frameworks (MOFs), which are constructed from metal clusters and organic linkers, have attracted considerable attention due to their high surface area, diverse structural topologies, well-defined pore structures and chemical properties.[1] MOFs have been employed in gas storage and separation,[2] catalysis,[3] sensing,[4] drug delivery[5] and biomedical field.[6] Particularly, increasing number of MOFs, including MIL-101,[7] ZIF-8,[8] UiO-66,[9,10] PCN-222 (ref. 11) and NU-1000,[12] are widely used as nanocarriers for drug delivery and theragnostic applications. These MOFs have been extensively studied because of their controllable pore size and composition, water stability, dispersibility and biodegradability. Among them MOFs, MILs (Materials Institute Lavoisier) are considered as promising nanocarriers because of iron(III) polycarboxylate for applications structures of particular promise. For example, MIL-based MOFs were first used as potential drug delivery systems by Férey *et al.* in 2006.[13] Horcajada *et al.* reported the synthesis of a series of porous iron(III) based MOFs, including MIL-100, 101, 89, 88A and 53, which were used as a carrier to load and release different types of drugs.[14]

In order to enhance the properties of MOFs in biomedical applications, the nano-size of nanoparticles, which could expose more active sites, remain stable and deliver drugs into the cells, is considered. Therefore, an accurate control of the particle size is mandatory in biological applications. The size of particles greater than 200 nm usually results in high toxicity to cells, thus reducing the drug delivery efficiency, while the size of particles lower than 200 nm exerts better transport capacity and distribution *in vivo*. Numerous different methods have been developed for fabricating monodisperse and crystalline nano-size MOFs by a range of techniques, including the sol-vothermal method,[15] reverse-phase microemulsion method,[16] ultrasonic synthesis,[17] surfactant-mediated hydrothermal synthesis[18,19] and microwave irradiation synthesis.[19,20] Although great advances have been reported in the synthesis of nanoscale MOFs, the understanding of size-biological property relation-ship of nano-MOFs is still a challenge in the precise control of the size and shape of MIL based MOFs. For example, the ultrasonication and irradiation approach allows for controlling the nucleation and crystallization processes by heating reaction mixtures under microwave irradiation.[14,17] However, by this method it is difficult to precisely control the particle size and shape of the resulting MIL nanocrystals. In addition, surfactant-mediated synthesis has been also proved to be an effective method for controlling the particle size and attracted much attention, because the surfactant molecules could be

[a]*Sanya Central Hospital (Hainan Third People's Hospital), Sanya, Hainan 572000, China. E-mail: chenjuan1227@126.com*

[b]*College of Chemistry and Chemical Engineering, Hunan University, Changsha, Hunan 410082, China*

† Electronic supplementary information (ESI) available. See DOI: 10.1039/d0ra09915e

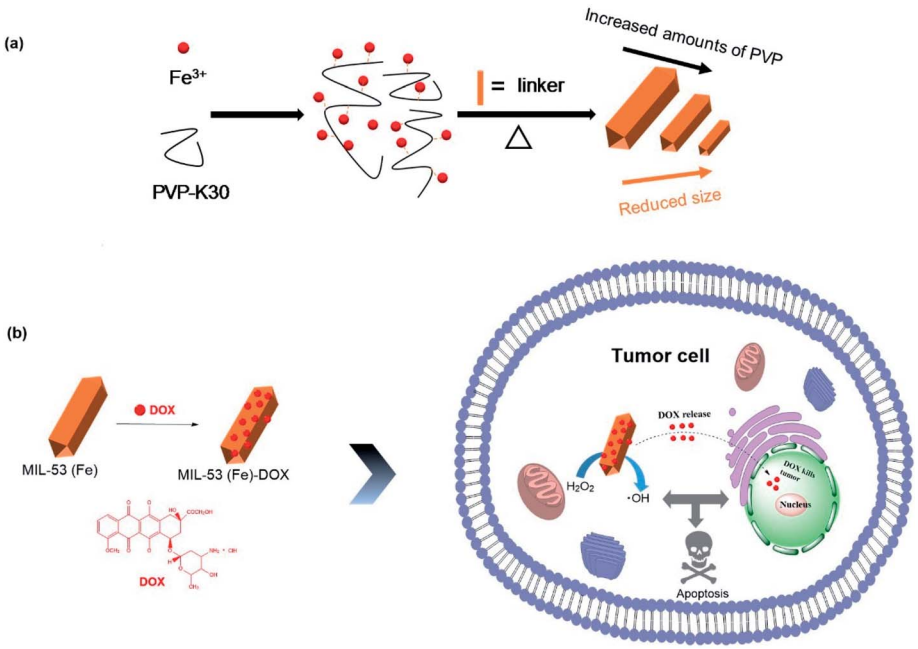

Scheme 1 Schematic illustration of the size-controlled fabrication of MIL-53(Fe) and enhancing antitumor effects. (a) Preparation of MIL-53(Fe) nanocrystals. (b) Preparation of MIL-53(Fe)$_{-200}$-DOX and chemodynamic therapy and chemotherapy.

coordinated weakly with metal ions to provide steric stabilization.[21] For example, Duong Duc La *et al.* synthesized nano-MIL-53 (Fe) functionalized with polyethylene glycol (PEG) by ultrasonication.[20] Although this method was simple and provided a controllable size, it was difficult to obtain nano-MIL-53 with good crystallinity. Trong-on Do *et al.* reported a new approach for the synthesis of nano-MIL-88B nanoparticles with a controlled size by adding a non-ionic surfactant polymer F127 in the synthetic mixture.[21,22] Some methods have achieved the synthesis of nanoscale Fe based MOFs by adding surfactant molecules, but monovalent capping ligands (F127) have not became the controlling agent to fabricate nano-MIL-53 (Fe). Therefore, size control of MOFs is an essential requirement in biological applications of nanoparticles, such as cancer therapy and drug delivery.

Reactive oxygen species (ROS) are a family of reactive chemical species containing oxygen, including hydrogen peroxide, hydroxyl radicals, superoxide and singlet oxygen.[23] ROS as important active molecules play a crucial role in cancer, neurodegenerative diseases and cardiovascular diseases.[24] ROS produced by nano-catalytic Fenton reactions were reported to be a new class of ROS-mediated anticancer therapeutics, which convert H_2O_2 into highly toxic $^{\cdot}OH$ by Fe.[25] In line with this phenomenon, a nanoscale ion-based metal–organic framework (NH_2-MIL-88B (Fe)) with intrinsic peroxidase like activity has been selected as a nano-catalytic medicine to trigger the therapeutic process. Other than nano-catalytic medicine, doxorubicin (DOX), a well-known broad-spectrum cancer drug, is clinically used to treat a variety of malignant tumors, such as breast cancer, solid tumors and leukemia.[26] Accordingly, the drug delivery as well as nano-catalytic ROS generation for combinatorial therapies for cancer has attracted more and more attention.

In this work, for the first time, we reported a new approach for the size-controlled synthesis of uniform iron(III)-based MIL-53 nanocrystals using the non-ionic surfactant PVP. In this approach, PVP plays a crucial role not only in controlling the size of the MIL-53 (Fe) nanocrystals but also in obtaining high crystallinity. A combinational therapeutic approach was presented for drug delivery and ROS therapy. The chemotherapy drug DOX was encapsulated into MIL-53(Fe) using a physisorption method. SEM, XRD, FTIR and TGA were used to characterize the MIL-53(Fe). For its application analysis, the cancer drug DOX was introduced into the MIL-53(Fe) by a physical adsorption method. H_2O_2 in the Fenton reaction was catalyzed into $^{\cdot}OH$ by Fe^{3+} that enables ROS mediated therapy. The combined efficiency of DOX release and ROS induction by MIL-53(Fe)-DOX was studied using 4T1 cells by CCK-8 and fluorescence imaging (Scheme 1).

Experimental section

Materials

Terephthalic acid ($C_6H_4(COOH)_2$, H_2BDC, 98%), ferric chloride hexahydrate ($FeCl_3 \cdot 6H_2O$, 98%) and polyvinylpyrrolidone K30 were obtained from Aladdin (Shanghai, China), and *N*,*N*-dimethylacetamide (DMA, 99%) was purchased from Hushi (Shanghai, China). 2′,7′-Dichlorodihydrofluorescein diacetate (H_2DCFDA) and doxorubicin hydrochloride (98%) were purchased from Macklin (Shanghai, China).

Characterization

The particle size and morphology of the sample were observed by Scanning Electron Microscopy (SEM, Hitachi S-4600) and Transmission Electron Microscopy (TEM). Powder X-ray

diffraction (XRD) patterns were recorded using a Bruker D8 Advance X-ray diffractometer with Cu Kα irradiation operated at 40 kV and 40 mA. Thermogravimetric analysis (TGA) was performed using a NETZSCH STA 449F3 simultaneous thermogravimetric analyzer from room temperature to 800 °C, with a heating rate of 10 °C min^{-1} under a nitrogen atmosphere. Fourier transform infrared spectra (FTIR) were recorded using a Nicolet iS50 FTIR spectrometer (Thermo Scientific) and UV-vis absorption spectra on a Shimadzu UV-3600 spectrophotometer. The zeta potential measurement of the samples dispersed in pure water was conducted using a Malvern Zetasizer Nano ZS90. Fe(III) content was determined using an Agilent 7900 inductively coupled plasma mass spectrometry (ICP-MS) system.

Preparation of MIL-53(Fe)

MIL-53(Fe) was prepared following the previous work.[27] The size-controlled synthesis of four samples of MIL-53(Fe) with different PVP contents was performed using a hydrothermal route. Typically, 41.5 mg of H_2BDC and 67.5 mg $FeCl_3 \cdot 6H_2O$ were dissolved in 10 mL bottles containing 30 mL of DMA with magnetic stirring for 10 minutes; thereafter, various contents (10, 50, 100 and 200 mg) of PVP were added into the mixture. The reaction mixture was transferred into an autoclave for crystallization. When the reaction was completed, the product was recovered and washed with DMA 3 times, followed by ethanol 3 times by centrifugation to remove the surfactant and excess reactants. The obtained samples were dried under vacuum conditions overnight before further characterization. All four prepared MIL-53(Fe) samples were fully characterized and the MIL-53(Fe) with the PVP content of 200 mg (MIL-53 $(Fe)_{-200}$) was used for drug delivery study.

DOX loading

0.8 mg mL^{-1} doxorubicin hydrochloride (DOX-HCl) aqueous solution (4 mL) was added into the aqueous solution of MIL-53 $(Fe)_{-200}$ and stirred for 72 h in the dark at room temperature. Finally, the products were washed with water five times by centrifugation to remove the free DOX. The concentration of DOX was calculated from the UV-vis spectra using a calibration formula of $Y = 23.05X + 0.0121$, where Y is the absorbance at 480 nm, and X is the concentration of DOX (μg mL^{-1}). To determine the DOX content of MIL-53(Fe), the absorbance contributed by MIL-53(Fe) was deducted prior to the calculation.

Release of DOX and Fe(III) ions from MIL-53 $(Fe)_{-200}$-DOX

In order to determine the release capability of the DOX-loaded MIL-53(Fe), 15 mg of the loaded materials (MIL-53(Fe)-DOX) were immersed in 3 mL water and phosphate buffer solutions of pH 6.0 and 7.4 at 37 °C and shaken in the dark for different periods (1 h, 2 h, 4 h, 8 h, 12 h, 24 h, 36 h, 48 h and 72 h). The amount of DOX release was calculated by measuring the absorbance of the release medium at 480 nm. The experiment was repeated 3 times.

The MIL53(Fe)-DOX in the dispersions was separated using a filter head (0.22 μm). Fe(III) ion concentration in the filtrate was measured by ICP-MS.

Detection of hydroxyl radical (·OH) production

The influence of pH on ·OH production in phosphate buffer solution (PBS) at two different pH values (7.4 and 5.2) was investigated. The detector 3,3′,5,5′-tetramethyl-benzidine (TMB) was applied to monitor the ·OH generation of MIL-53 $(Fe)_{-200}$-DOX. At different time periods, the absorbance was measured at 652 nm *via* a UV-vis spectrometer.

Cell culture

4T1 (mouse mammary carcinoma) cells were grown in Dulbecco's Modified Eagle Medium (DMEM) supplemented with 10% fetal bovine serum (FBS) and 100 U mL^{-1} penicillin and 1% streptomycin. The cells were cultured at 37 °C in 5% CO_2.

Cytotoxicity assay

4T1 cells cultured in 96-well plates (8000 cells per well) were treated with MIL-53 (Fe) and MIL53 (Fe)-DOX (containing the same content Fe(III) of different concentrations (3.12–50 μg mL^{-1})) for 24 h in culture medium. Similarly, the cells were also incubated for 24 h with different concentrations of DOX (0–15 μg mL^{-1}) of MIL53$(Fe)_{-200}$-DOX and free DOX. Then, the culture medium was removed and washed with PBS. Cell viability was measured using CCK-8 kit assay according to the manufacturer's instructions (Beyotime, China).

Cell imaging

4T1 cells were seeded in 6-well culture plates and cultured in DMEM for 24 h. Then, the MIL-53$(Fe)_{-200}$-DOX nanohybrids were added into the wells at a final DOX concentration of 3 μg mL^{-1}. After incubation for 3 h, the cells were washed three times with PBS and fixed with 1 mL of 4% paraformaldehyde in PBS for 10 min. Subsequently, the cells were washed twice with PBS again and stained with Hoechst 33342 dye (Beyotime, China) to mark the nucleus. Finally, the cells were imaged by CLSM (Olympus FV1000, Japan).

In vitro ·OH detection

The 4T1 cells were seeded in 6-well culture plates and cultured in DMEM for 24 h. Then, the free DOX, MIL-53$(Fe)_{-200}$ and MIL-53$(Fe)_{-200}$-DOX (DOX: 2 μg mL^{-1} and Fe(III): 6.64 μg mL^{-1}) were incubated for another 2 h. Then, 1 mL of H_2DCFDA (10 mM) (Beyotime, China) was added and incubated for 20 min. Finally, the cells were washed three times with PBS and fixed with 1 mL of 4% paraformaldehyde in PBS for 10 min. Subsequently, the cells were washed twice with PBS again and stained with Hoechst 33342 dye (Beyotime, China) to mark the nucleus. Finally, the cells were imaged by CLSM (Olympus FV1000, Japan).

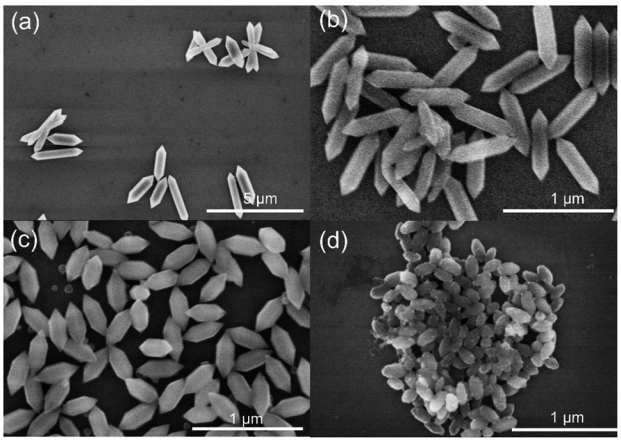

Fig. 1 SEM images of flexible MIL-53(Fe) fabricated with the PVP mass of (a) 0 mg, (b) 50 mg, (c) 100 mg and (d) 200 mg, respectively.

Results and discussion

Preparation and characterization of MIL-53(Fe)

Different stages of the synthesis of MIL-53(Fe) (i) without and (ii) with PVP in the synthetic mixture were studied to illustrate the role of PVP in controlling the size of MIL-53(Fe). Fig. 1 shows the Scanning Electron Microscopy (SEM) images of MIL-53(Fe) and MIL-53(Fe)$_{-200}$ samples prepared without and with the surfactant PVP. As shown in Fig. 1a, under synthesis conditions without PVP, the MIL-53(Fe) microcrystals were produced from an aqueous reaction mixture of Fe^{3+} and H_2BDC, with an average length of 2.2 μm and a width of 0.49 μm. Interestingly, in the presence of PVP, the particle size decreased from micro- to nanometers and the morphology still remained unchanged under the same synthetic conditions. Furthermore, the crystal sizes of MIL-53(Fe) were optimized by tuning the PVP concentration (Fig. 1b–d). It was obvious that adjusting the concentration of PVP could control the size of MIL-53(Fe) nanocrystals in the synthetic mixture. When the concentration of PVP was increased to 50 mg, 100 mg and 200 mg, respectively, a significant change in the size of MIL-53(Fe) nanocrystals was found; in addition, the average sizes of the nanocrystals were 600 ± 30 nm, 380 ± 54 nm and 190 ± 22 nm in length and 140 ± 14, 240 ± 15 and 100 ± 12 nm in width, respectively. The reason why the crystal sizes reduced gradually with increasing PVP concentration could be explained by the effects of the PVP droplet during the nucleation of MIL-53(Fe) that PVP, as a nanoreactor, controls the growth of the crystal nucleus. At low amount of PVP, little nucleation of crystals occurred, causing the size of MIL-53(Fe) to remain almost unchanged. As the PVP concentration was increased, more MIL-53(Fe) nucleation occurred, and the size of the obtained MIL-53 (Fe) crystals was significantly decreased. These results indicate that the PVP surfactant plays an important role in the preparation of MIL-53(Fe) nanocrystals. All the above results indicated that the small size MIL-53(Fe) nanocrystals were successfully prepared and could be used for further application.

XRD was performed to determine the crystalline structures of the prepared MIL-53(Fe) with and without the assistance of PVP. As shown in Fig. 2, the main diffraction peaks at 9.17, 9.56 and 10.58 were observed clearly. And all the diffraction peaks are in good agreement with the diffraction peaks of MIL-53(Fe) reported in previous works.[27]

FTIR spectroscopy was employed to determine the characteristic peaks and molecular structure of the MIL-53(Fe) and MIL-53(Fe)$_{-200}$ nanocrystals. Fig. 3 shows the IR spectra of the nanocrystal samples prepared in the presence of both PVP and H_2BDC linker. The broad band at 3000 cm^{-1} in the FTIR spectrum of the H_2BDC linker was the characteristic region of the COOH group. In the spectra of MIL-53(Fe) and MIL-53(Fe)$_{-200}$, the characteristic peaks in the region of 1400–1700 cm^{-1} corresponded to the carbonyl group (1680 cm^{-1}) units and the stretching vibration of the carboxyl groups with the Fe(III) metal nodes (1579 cm^{-1}).[28] In addition, the absorption peak was observed at 535 cm^{-1} due to the formation of the Fe–O band, which confirmed the coordination between Fe(III) metal nodes and carboxylic groups of the H_2BDC linker. A weak peak at

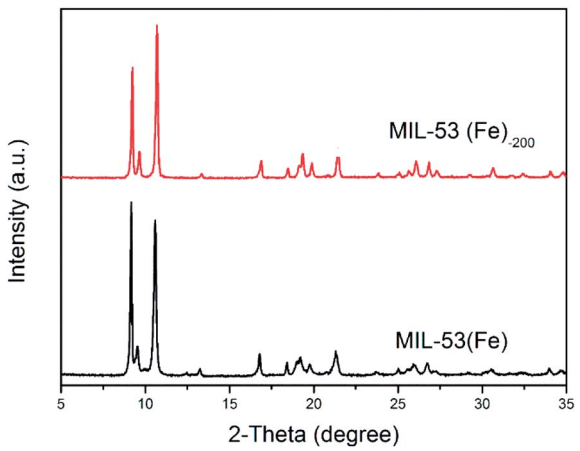

Fig. 2 XRD patterns for MIL-53(Fe) nanocrystal samples synthesized with 200 mg of PVP powder without (black curve) and with (red curve) surfactant PVP assistance.

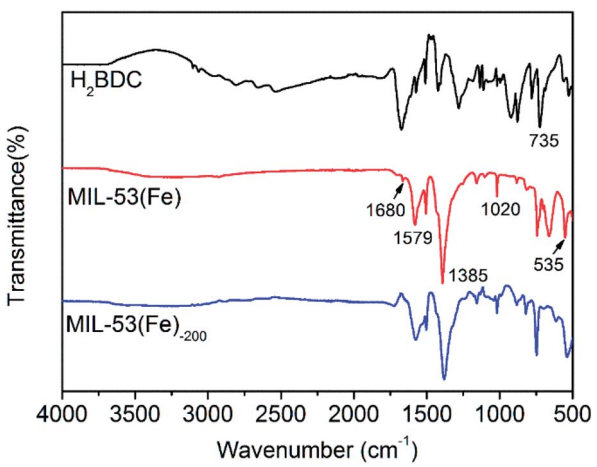

Fig. 3 FTIR spectra of the H_2BDC compound (black curve), MIL-53(Fe) (red curve) and the MIL-53(Fe)$_{-200}$ (blue curve).

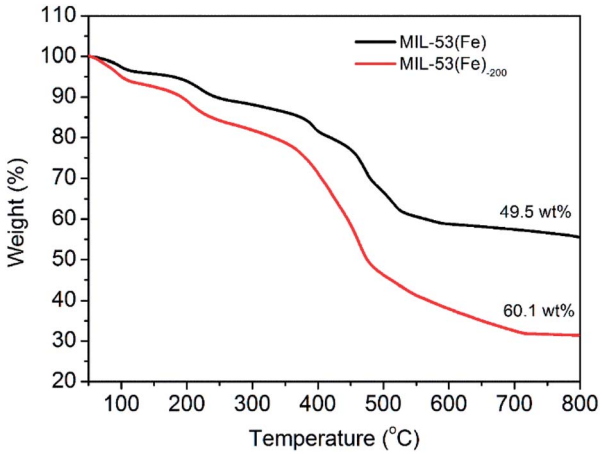

Fig. 4 TGA curves of MIL-53(Fe) (black curve) and the MIL-53(Fe)$_{-200}$ (red curve) under nitrogen.

1727 cm^{-1} was observed in the spectrum of MIL-53 (Fe), indicating the presence of the free H_2BDC ligand in the nanoscale MOF crystals. In general, the samples of MIL-53(Fe) and MIL-53(Fe)$_{-200}$ nanocrystals exhibit similar FTIR spectra.

The amounts of organic components of MIL-53(Fe) and MIL-53(Fe)$_{-200}$ nanocrystals were quantified by TGA under N_2 at 10 °C min^{-1}. As shown in Fig. 4, the two nanocrystals exhibited a small weight loss below 200 °C, indicating the escape of occluded water molecules. For MIL-53(Fe), the TGA curves showed a major weight loss (approximately 49.5 wt%) in the range of 200–600 °C, indicating that the H_2BDC ligand of MIL-53(Fe) was removed. As for MIL-53(Fe)$_{-200}$, the first weight loss was higher than that of MIL-53(Fe) in the range of 200–400 °C, which might be attributed to the PVP surfactant, implying the presence of the PVP surfactant in the materials. The second weight loss happened at 400–600 °C, and the weight percentage of PVP in MIL-53 was calculated to be 10.6 wt%. Based on the data, the weight ratio of H_2BDC ligand : PVP surfactant in MIL-53(Fe)$_{-200}$ nanocrystals was calculated to be 47 : 10.

The MIL-53(Fe) nanocrystals have a suitable particle size and a Fenton reaction catalyst, exerting great potential for anticancer drug delivery and ROS dynamic therapy *in vitro*. DOX is known as a widely applied anticancer drug for the treatment of several cancers, including breast cancer, solid tumors and leukemia. Therefore, MIL-53(Fe) nanocrystals could be used as a drug nanocarrier for DOX loading and release. Fig. 5a shows the FTIR spectra of MIL-53(Fe)$_{-200}$ and MIL-53(Fe)$_{-200}$-DOX nanocrystals. Compared with the characteristic peaks of MIL-53(Fe)$_{-200}$ mentioned above, the absorption peaks at 1580 cm^{-1} and 1627 cm^{-1} in the spectrum of MIL-53(Fe)$_{-200}$-DOX were attributed to the C=C stretching vibration of the aromatic ring on DOX, indicating that DOX was successfully loaded on the MIL-53(Fe)$_{-200}$. The loading of DOX into MIL-53(Fe)$_{-200}$ nanocrystals was further confirmed using UV-vis absorbance spectra. As shown in Fig. 5b, the MIL-53(Fe)$_{-200}$ nanocrystals showed an absorption peak at 260 nm and 340 nm. An absorption peak (487 nm) was also observed in the spectrum of MIL-53(Fe)$_{-200}$-DOX belonging to DOX, which was similar to the absorption peak wavelength of free DOX, indicating the successful loading of DOX into MIL-53(Fe)$_{-200}$ nanocrystals. Additionally, zeta

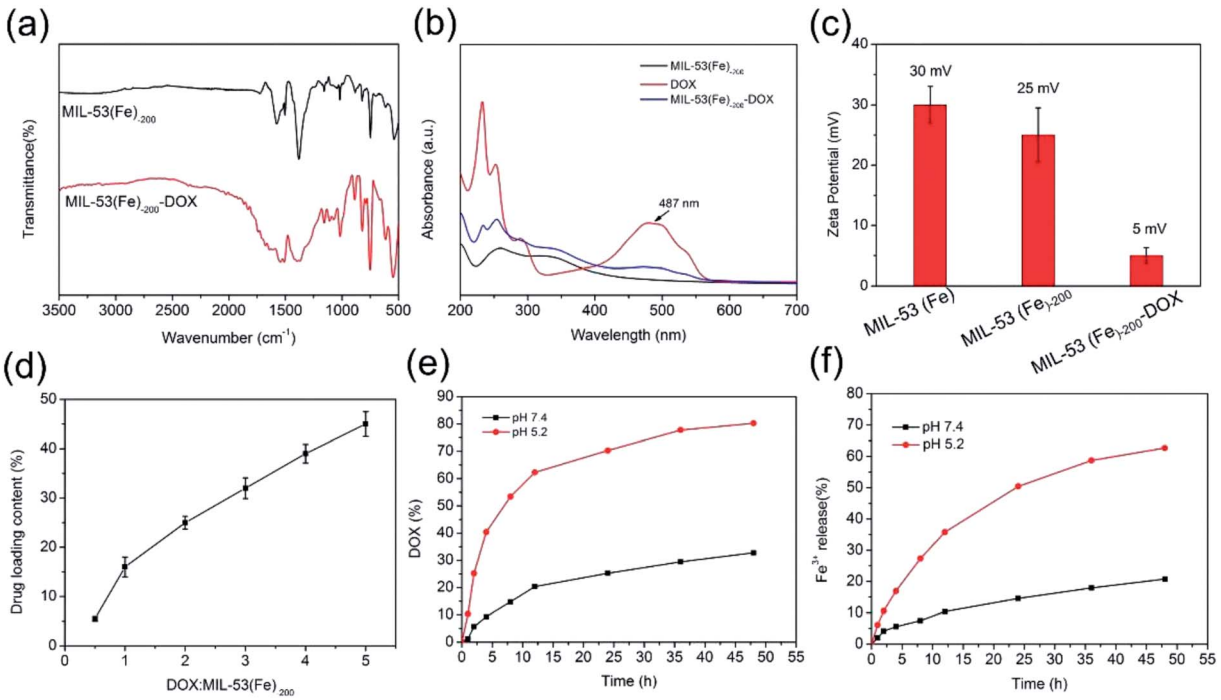

Fig. 5 (a) FT-IR spectra; (b) UV-vis absorbance spectra and (c) zeta potentials of MIL-53(Fe), MIL-53(Fe)$_{-200}$ and MIL-53(Fe)$_{-200}$-DOX; (d) drug loading content under different MIL-53(Fe)$_{-200}$ mass ratios; *in vitro* DOX and Fe(III) release of (e) MIL-53(Fe)$_{-200}$-DOX and (f) MIL-53(Fe)$_{-200}$ at pH 5.2 and 7.4, respectively.

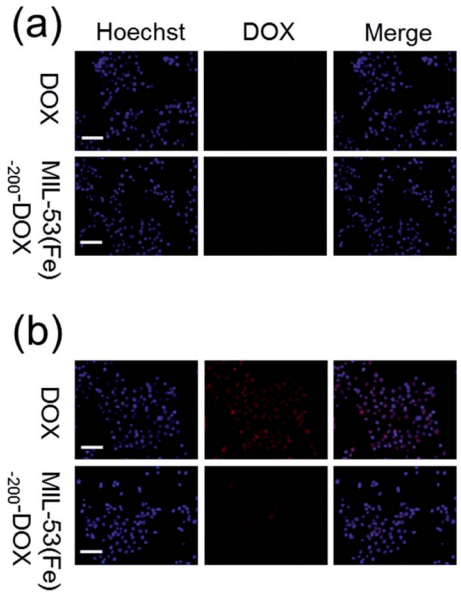

Fig. 6 Fluorescence images of 4T1 cells treated with DOX and MIL-53(Fe)$_{-200}$-DOX for (a) 1 h and (b) 2 h (scale bar: 50 μm).

potential measurements (Fig. 5c) revealed that the potential of the MIL-53(Fe)$_{-200}$ gradually decreased after the loading of DOX, confirming that the MIL-53(Fe)$_{-200}$-DOX was successfully prepared.

The DOX loading content of MIL-53(Fe)$_{-200}$ is shown in Fig. 5d. A gradual increment in the loading content of DOX was obtained with the increase of the initial DOX concentration. With the increase of the DOX:MIL-53(Fe)$_{-200}$ mass ratio, the mass drug-loading rate was calculated to be approximately 45% at a mass ratio of 5. The release of DOX from the drug loaded MIL-53(Fe)$_{-200}$-DOX *in vitro* was investigated under different physiological environments. The drug release experiments were performed in a simulated human microenvironment including blood (pH = 7.4) and tumor cell endosomes and lysosomes (pH = 5.2). As shown in Fig. 5e, a sharp increase of DOX release rates from MIL-53(Fe)$_{-200}$ nanocarriers was observed when the pH of the release medium was lowered from 7.4 to 5.2. More interestingly, 80.25% of DOX within 72 h was released at pH 5.2, while only 32.77% of DOX was released at pH 7.4. This release behavior can be attributed to the protonation of the amino group of DOX at a lower pH value.[29,30] Therefore, the MIL-53(Fe)$_{-200}$-DOX was proved to be pH-sensitive by reducing DOX leakage during blood circulation and yet releasing a sufficient amount of DOX under the acidic condition, achieving cancer-targeted DOX delivery. This selective release is beneficial for cancer therapy while lessening normal tissue toxicity.[31] These results indicated that the specific interactions between the skeletons of the MIL-53(Fe)$_{-200}$ and the drug molecules not only prolonged the release process but also enhanced the loading capacity.

Meanwhile, the Fe^{3+} release as a result of pH-responsive MIL-53(Fe)$_{-200}$-DOX degradation was investigated using ICP-MS (Fig. 5f). Compared with the Fe^{3+} release under pH 5.2, the Fe^{3+} release ratio was much higher than at pH 7.4, where an ultimate release ratio of 2.75% at pH 7.4 and 63.72% at pH 5.2 were recorded under the same conditions for 72 h. These results demonstrated that the degradation rate speeded up under more acidic conditions.[32]

Cellular uptake, ROS detection and cytotoxicity assay *in vitro*

After the cellular uptake and drug release were observed, 4T1 cells were treated with MIL-53(Fe)$_{-200}$-DOX, and then the red fluorescence was analyzed using fluorescence images. As shown in Fig. 6, cell nuclei were labeled with Hoechst (blue), while DOX was marked with red fluorescence. Red fluorescence was observed in the cells after different treatments, suggesting that the free DOX and MIL-53(Fe)$_{-200}$-DOX nanocrystals could enter 4T1 cells after co-incubation with 4T1 cells, and DOX was then released from the MIL-53(Fe)$_{-200}$-DOX nanoparticles in the cells. And there was no red fluorescence in the 4T1 cells after MIL-53(Fe)$_{-200}$ treatment under the same Fe ion conditions (Fig. S1†). It was found that the red fluorescence intensities were higher at 2 h compared to those at 1 h in 4T1 cells, confirming that the DOX release behavior in the 4T1 cells was time-dependent.

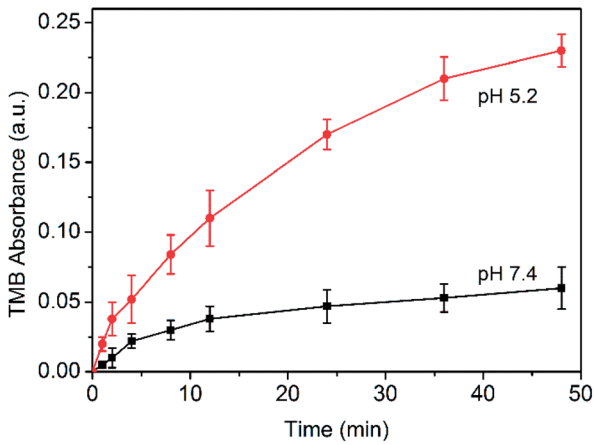

Fig. 7 Detection of $^{\bullet}OH$ generation in an H^+ enhanced tumor environment (around pH = 5.2).

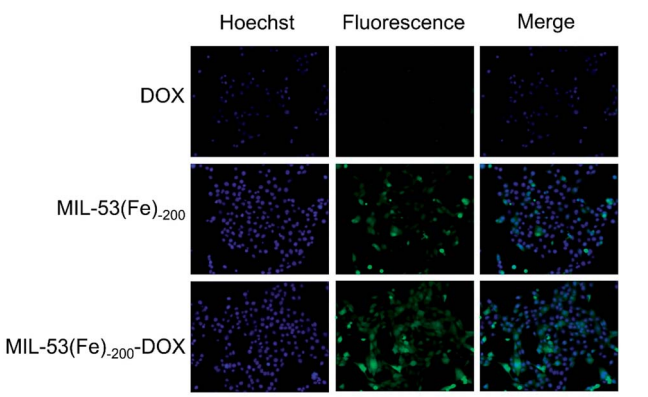

Fig. 8 Evaluation of ROS levels with a fluorescence microscope. (Scale bar: 50 μm).

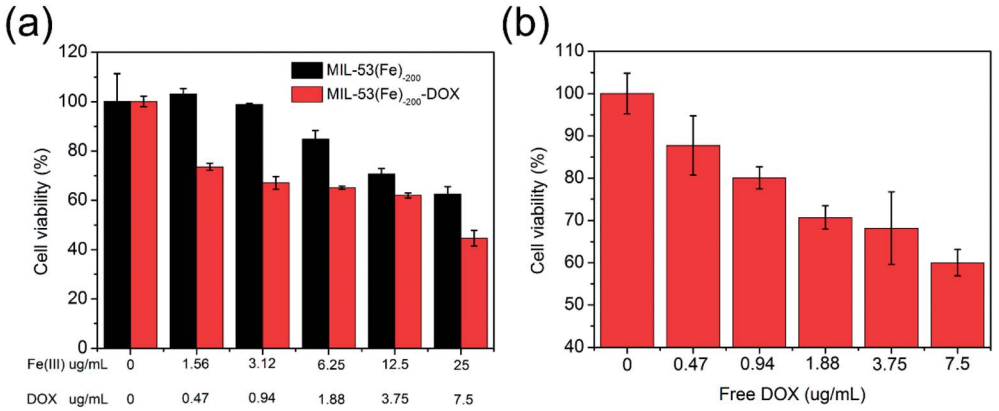

Fig. 9 The viability of 4T1 cells after incubation with various concentrations of MIL-53 (Fe)$_{-200}$-DOX (a) and free DOX (b) for 24 h.

$^{\bullet}$OH, as a member of reactive oxygen species (ROS), plays an important role in oncotherapy by inducing oxidative damage to lipids, DNA, RNA, and proteins.[33] To detect the generation of $^{\bullet}$OH at different pH, MIL-53(Fe)$_{-200}$-DOX was compared with 3,3′,5,5′-tetramethyl-benzidine (TMB), which was used as a specific $^{\bullet}$OH indicator. In Fig. 7, the MIL-53(Fe)$_{-200}$-DOX showed a higher TMB absorbance at pH 5.2 compared to pH 7.4, indicating that the production of $^{\bullet}$OH increased with the decrease of pH by facilitating the occurrence of reactions mediated by H^+.[34] Considering that H_2O_2 could be catalyzed by MIL-53(Fe)$_{-200}$ to generate $^{\bullet}$OH *via* a Fenton-like reaction, the fluorescence images were obtained to observe the generation of $^{\bullet}$OH by the H_2DCFDA probe. Furthermore, the ROS generation capabilities of free DOX, MIL-53(Fe)$_{-200}$ and MIL-53(Fe)$_{-200}$-DOX *in vitro* were measured by observing the green fluorescence. As shown in Fig. 8, the green fluorescence of the H_2DCFDA probe in MIL-53(Fe)$_{-200}$-DOX was stronger than that of single free DOX and MIL-53(Fe)$_{-200}$. These results indicated that the co-treatment with DOX and MIL-53(Fe)$_{-200}$ could significantly increase ROS levels in cancer cells, making it a potent anti-cancer strategy.

To further evaluate the toxicity of the nanodrug, the cytotoxicity of MIL-53(Fe)$_{-200}$ and MIL-53(Fe)$_{-200}$-DOX was evaluated by using the CCK-8 assay with 4T1 cells (Fig. 9). With the increase of MIL-53(Fe)$_{-200}$ concentration within 0–25 μg mL^{-1}, the cell viability was reduced to about 62.5% due to the effects of ROS-mediated therapy. In contrast, MIL-53(Fe)$_{-200}$-DOX nanodrug ROS-mediated/chemo-therapy caused a higher toxicity (cell viability of 44.7%) compared with MIL-53(Fe)$_{-200}$ (Fig. 9a). In addition, as shown in Fig. 9b, after incubation with free DOX (0–7.5 μg mL^{-1}) for 24 h, the cell viability was lower than that of MIL-53(Fe)$_{-200}$-DOX (containing the same DOX dosage as MIL-53(Fe)$_{-200}$-DOX). The results showed that MIL-53(Fe)$_{-200}$ nanocrystals may be a potential drug carrier to efficiently deliver DOX into cancer cells for ROS-mediated/chemo-therapy.

Conclusions

In summary, a new route was developed for the successful synthesis of MIL-53(Fe) nanocrystals with controlled sizes using the non-ionic surfactant PVP in the synthetic mixture. As the concentration of PVP increases, a lower rate of nucleation and crystal growth was generated, and significantly decreased, nano-size of the obtained MIL-53(Fe) crystals were obtained. The MIL-53(Fe)$_{-200}$ nanocrystals in the presence of a PVP mass of 200 mg showed nano-sizes with approximately 190 nm in length and 100 nm in width. The MIL-53(Fe) showed a high loading rate of the anticancer drug DOX and high release rate of the DOX under *in vitro* conditions; 45% of the drug was released after 72 h. The H_2O_2 generated was catalyzed by Fe^{3+} into $^{\bullet}$OH to enable ROS-mediated dynamic therapy. MIL-53(Fe)$_{-200}$ nanocrystals may be a potential drug carrier to efficiently deliver DOX into cancer cells for ROS-mediated dynamic/chemo-therapy. This work provided a new route for the preparation of multi-functional nanoplatforms for cancer treatment in practical applications by effective delivery of drugs.

Conflicts of interest

There are no conflicts to declare.

Acknowledgements

This work was supported by Medical Health Science and Technology Innovation Project of Sanya City (No. 2019YW13).

References

1 S. L. James, *Chem. Soc. Rev.*, 2003, **32**, 276–288.
2 Z. Zhang, S. B. Peh, Y. Wang, C. Kang, W. Fan and D. Zhao, *Angew. Chem., Int. Ed.*, 2020, **59**, 18927–18932.
3 A. H. Chughtai, N. Ahmad, H. A. Younus, A. Laypkov and F. Verpoort, *Chem. Soc. Rev.*, 2015, **44**, 6804–6849.
4 R. Hu, X. Zhang, K.-N. Chi, T. Yang and Y.-H. Yang, *ACS Appl. Mater. Interfaces*, 2020, **12**, 30770–30778.
5 T. Xue, C. Xu, Y. Wang, Y. Wang, H. Tian and Y. Zhang, *Biomater. Sci.*, 2019, **7**, 4615–4623.
6 T. Zhang, Z. Jiang, L. Chen, C. Pan, S. Sun, C. Liu, Z. Li, W. Ren, A. Wu and P. Huang, *Nano Res.*, 2020, **13**, 273–281.

7 J. Wang, D. Chen, B. Li, J. He, D. Duan, D. Shao and M. Nie, *Sci. Rep.*, 2016, **6**, 26126.
8 L. Zhang, Y. Gao, S. Sun, Z. Li, A. Wu and L. Zeng, *J. Mater. Chem. B*, 2020, **8**, 1739–1747.
9 I. Abánades Lázaro, C. J. R. Wells and R. S. Forgan, *Angew. Chem., Int. Ed.*, 2020, **59**, 5211–5217.
10 X. Gao, R. Cui, G. Ji and Z. Liu, *Nanoscale*, 2018, **10**, 6205–6211.
11 X. Leng, H. Huang, W. Wang, N. Sai, L. You, X. Yin and J. Ni, *J. Evidence-Based Complementary Altern. Med.*, 2018, **2018**, 3249023.
12 J. W. M. Osterrieth and D. Fairen-Jimenez, *Biotechnol. J.*, 2020, 2000005.
13 P. Horcajada, C. Serre, M. Vallet-Regí, M. Sebban, F. Taulelle and G. Férey, *Angew. Chem.*, 2006, **118**, 6120–6124.
14 P. Horcajada, T. Chalati, C. Serre, B. Gillet, C. Sebrie, T. Baati, J. F. Eubank, D. Heurtaux, P. Clayette, C. Kreuz, J.-S. Chang, Y. K. Hwang, V. Marsaud, P.-N. Bories, L. Cynober, S. Gil, G. Férey, P. Couvreur and R. Gref, *Nat. Mater.*, 2010, **9**, 172–178.
15 M. Rezaei, A. Abbasi, R. Varshochian, R. Dinarvand and M. Jeddi-Tehrani, *Artif. Cells, Nanomed., Biotechnol.*, 2018, **46**, 1390–1401.
16 W. J. Rieter, K. M. L. Taylor, H. An, W. Lin and W. Lin, *J. Am. Chem. Soc.*, 2006, **128**, 9024–9025.
17 L.-G. Qiu, Z.-Q. Li, Y. Wu, W. Wang, T. Xu and X. Jiang, *Chem. Commun.*, 2008, 3642–3644, DOI: 10.1039/B804126A.
18 T. Uemura and S. Kitagawa, *J. Am. Chem. Soc.*, 2003, **125**, 7814–7815.
19 N. Khan, I. Kang, H. Seok and S. Jhung, *Chem. Eng. J.*, 2011, **166**, 1152–1157.
20 H. P. Nguyen Thi, H. D. Ninh, C. V. Tran, B. T. Le, S. V. Bhosale and D. D. La, *ChemistrySelect*, 2019, **4**, 2333–2338.
21 M.-H. Pham, G.-T. Vuong, A.-T. Vu and T.-O. Do, *Langmuir*, 2011, **27**, 15261–15267.
22 B. Yang, L. Ding, H. Yao, Y. Chen and J. Shi, *Adv. Mater.*, 2020, **32**, 1907152.
23 B. D'Autréaux and M. B. Toledano, *Nat. Rev. Mol. Cell Biol.*, 2007, **8**, 813–824.
24 B. C. Dickinson and C. J. Chang, *Nat. Chem. Biol.*, 2011, **7**, 504–511.
25 B. Yang, Y. Chen and J. Shi, *Chem. Rev.*, 2019, **119**, 4881–4985.
26 T. D. Shenkenberg and D. D. Von Hoff, *Ann. Intern. Med.*, 1986, **105**, 67–81.
27 F. Millange, C. Serre, N. Guillou, G. Férey and R. I. Walton, *Angew. Chem., Int. Ed.*, 2008, **47**, 4100–4105.
28 R. Liang, F. Jing, L. Shen, N. Qin and L. Wu, *J. Hazard. Mater.*, 2015, **287**, 364–372.
29 W. Lin, X. Zhang, L. Qian, N. Yao, Y. Pan and L. Zhang, *Biomacromolecules*, 2017, **18**, 3869–3880.
30 Y.-I. Jeong, S.-G. Jin, I.-Y. Kim, J. Pei, M. Wen, T.-Y. Jung, K.-S. Moon and S. Jung, *Colloids Surf., B*, 2010, **79**, 149–155.
31 T. Sun, M. Zheng, Z. Xie and X. Jing, *Mater. Chem. Front.*, 2017, **1**, 354–360.
32 D. Wang, J. Zhou, R. Chen, R. Shi, G. Xia, S. Zhou, Z. Liu, N. Zhang, H. Wang, Z. Guo and Q. Chen, *Biomaterials*, 2016, **107**, 88–101.
33 S. S. Sabharwal and P. T. Schumacker, *Nat. Rev. Cancer*, 2014, **14**, 709–721.
34 M. Huo, L. Wang, Y. Chen and J. Shi, *Nat. Commun.*, 2017, **8**, 357.